

OLD DOMINION UNIVERSITY RESEARCH FOUNDATION

SCHOOL OF ENGINEERING  
OLD DOMINION UNIVERSITY  
NORFOLK, VIRGINIA

Technical Report 75-C1

(NASA-CR-142261) THE EFFECT OF SHEARING  
STRAIN-RATE ON THE ULTIMATE SHEARING  
RESISTANCE OF CLAY Final Technical Report  
(Old Dominion Univ., Norfolk, Va.) 40 p HC  
\$3.75 CACL 08M G3/42 N75-19772  
Unclas 13445

THE EFFECT OF SHEARING STRAIN-RATE ON THE  
ULTIMATE SHEARING RESISTANCE OF CLAY

*By*

Robert Y.K. Cheng

*Prepared for the*  
National Aeronautics and Space Administration  
Langley Research Center  
Hampton, Virginia

*Under*  
Grant No. NGL 47-003-012

March 1975



THE EFFECT OF SHEARING STRAIN-RATE ON THE  
ULTIMATE SHEARING RESISTANCE OF CLAY

*FINAL TECHNICAL REPORT*

*By*

Robert Y.K. Cheng

*Prepared for the*  
National Aeronautics and Space Administration  
Langley Research Center  
Hampton, Virginia 23665

*Under*  
Grant No. NGL 47-003-012

School of Engineering  
Old Dominion University  
Technical Report 75-C1

*Submitted by the*  
Old Dominion University Research Foundation  
P.O. Box 6173  
Norfolk, Virginia 23508

March 1975



## CONTENTS

	<u>page</u>
ABSTRACT . . . . .	1
INTRODUCTION . . . . .	2
LIST OF SYMBOLS . . . . .	2
PRESENT STATE OF KNOWLEDGE . . . . .	4
GENERAL THEORY . . . . .	5
TORSION TEST METHOD . . . . .	8
A. Torsion Apparatus . . . . .	8
B. Sample Preparation Unit and Procedure . . . . .	9
C. Testing Procedure . . . . .	11
ANALYSIS OF DATA . . . . .	12
SUMMARY AND CONCLUSIONS . . . . .	16
ACKNOWLEDGMENT . . . . .	16
REFERENCES . . . . .	17
APPENDIX . . . . .	18

## TABLES

Table		Page
1	Water content at various locations on a typical sample . . . . .	20
2	Values of coefficient $\alpha$ and $\beta$ at various dry density. . . . .	20

## Figures

Figure		
1	Reference axes and stress system . . . . .	21
2	Torsion apparatus . . . . .	22
3	Photograph of torsion apparatus . . . . .	23
4	Photograph of sample preparation unit . . . . .	24
5	Photograph of test samples . . . . .	25
6	Photograph of sample in triaxial cell . . . . .	26
7	Grain size distribution of clay . . . . .	27
8	Compaction property of clay . . . . .	28
9	Photographs of typical recorded time histories . . . . .	29
10	Dynamic response due to inertia of the torque sensing system . . . . .	32
11	Plot of shearing stress versus strain-rate . . . . .	33
12	Relationship between coefficient $\alpha$ and mean water content . . . . .	35
13	Plot of strain-rate versus $\log(\alpha - \tau)$ . . . . .	35
14	Newtonian and non-Newtonian viscosity, and plot of apparent viscosity versus strain-rate . . . . .	36

THE EFFECT OF SHEARING STRAIN-RATE ON THE  
ULTIMATE SHEARING RESISTANCE OF CLAY

By

Robert Y.K. Cheng<sup>1</sup>

ABSTRACT

This report describes a new approach to investigate the shearing resistance of cohesive soils subjected to a high rate of shearing strain. A fast step-loading torque apparatus was used to induce a state of pure shear in a hollow cylindrical soil specimen. The relationship between shearing resistance and rate of shear deformation was established for various soil densities expressed in terms of initial void ratio or water content.

For rate of shearing deformation studies to date, the shearing resistance increases initially with shearing velocity, but subsequently reaches a terminal value as the shearing velocity increases. The terminal shearing resistance is also found to increase as the density of the soil increases.

The results of this investigation are useful in the rheological study of clay. It is particularly important for mobility problems of soil runways, since the soil resistance is found to be sensitive to the rate of shearing.

---

<sup>1</sup> Professor of Engineering, Old Dominion University,  
Norfolk, Virginia 23508.

## INTRODUCTION

The objective of this study is to present a method for studying the effect of shearing strain-rate on the shearing resistance of cohesive soils. An experimental method was developed for measuring dynamic soil properties that can be applied to an analytic method for solving the problem of aircraft landings on soil runways. Currently the interest in operating an aircraft on unpaved landing sites has increased. Also in the case of overshooting a paved runway in an emergency, the aircraft will be subjected to stresses similar to operation on a substandard landing site. As the weight of the aircraft and landing speed increases, the aircraft, and in particular the landing gear, must be adequately designed in order to permit safe aircraft operations on unpaved sites.

Considerable studies have been performed (refs. 1, 2, and 3, for example) to measure the soil-tire interactions at ground speeds associated with small aircraft operations. The variables of these studies have included forward speed, tire inflation pressure, surface roughness, and soil strength. No rational explanation has yet been found to predict the soil-tire interaction. A recent analytic work (ref. 4) has shown qualitatively the correlation between the drag coefficient and velocity using soil properties obtained statically. Inevitably, all rational studies of the soil-tire interaction problem will require a description of the interface-stress distribution between the tire and soil. The ruts created by the tires of aircraft operating on certain soils serve as evidence to the large movement of soil masses.

## LIST OF SYMBOLS

$\alpha$	rheological coefficient describing the maximum ultimate shearing resistance
$\beta$	rheological coefficient
$\bar{\sigma}$	hydrostatic (spherical) stress tensor

$\bar{\epsilon}$	strain tensor
$\epsilon$	strain
$\bar{\dot{\epsilon}}$	strain-rate tensor
$\dot{\epsilon}$	strain-rate
$\bar{\tau}$	deviatoric stress tensor
$\sigma$	normal stress
$\sigma_m$	mean normal stress
$\tau$	shear stress
$\tau_{\max}$	maximum shear stress
$\dot{\gamma}$	shearing strain-rate
$\mu$	modulus of rigidity
$\eta$	non-Newtonian viscosity
$\eta_{\text{app}}$	apparent viscosity
$\phi$	angular rotation of top of sample
$h$	height of sample
$r$	radius of sample
$t$	time
$T$	torque
$w$	water content

Subscripts

$r, \theta, z$	directions in cylindrical coordinates
$11, 22, 33$	diagonal elements of stress tensor
$1, 2$	inside and outside radius of sample

Superscripts

"	spherical stress tensor
'	deviatoric stress tensor

## PRESENT STATE OF KNOWLEDGE

The stress-strain behavior of soils is influenced by the density, drainage condition, stress history, loading path, and rate of loading. It is evident that to establish a single constitutive equation for the stress-strain relationship of soils is an enormous task. The stability analysis for problems in geotechnical engineering is concerned with the failure concept in which the soil is treated as a rigid plastic solid. Defining the failure state of the soil as a state of stress at which a small increment of stress will induce a relatively large increment of strain, the strength parameters measured under gradually applied or static loads are the cohesion,  $c$ , and the angle of internal friction,  $\phi$ . With the density and all physical constituents of the soil remaining constant, the strength parameters of a soil can vary considerably with the drainage condition which induces pore water pressure in the soil. This phenomenon has brought about the common expression that the strength parameters are merely coefficients of the drainage condition of the soil under the given state of loading. Although the deformation characteristics and the influence of pore pressure on the effective strength of soils have been extensively studied (ref. 5), the general solution is still lacking for solving the forces and displacements in a soils engineering problem. However, the current knowledge in strength studies permits engineers to design and successfully build a wide variety of complex foundations and earth structures.

In recent years extensive investigations on dynamic soil properties have been conducted for problems related to foundation vibrations, earthquake-induced ground motions, and blast effects (ref. 6). These studies were only concerned with either small amplitude vibratory phenomena or stress levels up to failure. The parameters adopted for the studies are independent of rate effects. Since large movements of soil mass at high speed occur during aircraft landing, the soil properties required for drag and sinkage studies must depend upon the rate of loading or rate of deformation.

The shearing resistance and inertia of the soil contribute to the forces encountered in large soil displacements. The effect of rate of shearing deformation on the resistance of soils has been investigated for the earth penetration problem (ref. 7), and for the earth movement and tillage problem (ref. 8). For an experimental procedure that would subject the soil specimen to large strains, the state of stress developed in the specimen would become rather complex, and the test results would be difficult to interpret. By using a hollow cylindrically-shaped specimen (refs. 9 and 10), a state of pure shear exists within the specimen even at progressively large deformations. Since the geometric form of the specimen can be preserved throughout the test duration, the state of stress of the soil may be correlated with the strain in order to establish a shearing-stress strain-rate relationship. Guided by the above considerations, a torsion test procedure for a hollow cylindrical specimen was developed in this study.

#### GENERAL THEORY

The total state of stress, strain, or strain-rate in the soils may be decomposed into the hydrostatic (or spherical) state of stress and the deviatoric state of stress, so that

$$\begin{aligned}\bar{\sigma} &= \bar{\sigma} + \bar{\tau} \\ \bar{\epsilon} &= \bar{\epsilon}'' + \bar{\epsilon}' \\ \bar{e} &= \bar{e}' + \bar{e}'\end{aligned}$$

The hydrostatic stress tensor is described by the mean of the normal stress components as

$$\bar{\sigma} = \begin{bmatrix} \sigma_m & 0 & 0 \\ 0 & \sigma_m & 0 \\ 0 & 0 & \sigma_m \end{bmatrix} \quad \text{where } \sigma_m = \frac{1}{3} (\sigma_{11} + \sigma_{22} + \sigma_{33})$$

The hydrostatic stress tensor relates to the hydrostatic strain tensor which describes the deformation due to volume change, whereas the deviatoric stress tensor relates to the deviatoric strain tensor which describes the deformation due to shearing stresses.

Restricting this study to saturated cohesive soils, which will be treated as isotropic and incompressible, the equation of state for the elastic stress-strain relation due to shearing stress is

$$\tau = 2\mu \epsilon \quad (1)$$

For soils, the modulus of rigidity is not a constant, but is a function of the mean normal stress,  $\sigma_m$ . The equation of state for the plastic stress-strain relation due to shearing stresses may be expressed as

$$\tau = 2\eta \epsilon \quad (2)$$

known as the rheological equation of state for clay. For soils, the flow parameter  $\eta$  is not a constant, but is a function of many variables including the mean normal stress and shearing strain-rate. When the deformations are large, the work expended in elastic deformation is relatively insignificant in comparison with the work spent in plastic deformation for a hollow cylinder in torsion. The elastic resistance of the soil will be neglected so that all deformations are due to plastic work.

The state of stress of a hollow cylinder in torsion about the z axis (see fig. 1) under a confining pressure,  $\sigma_m$ , is

$$\bar{\sigma} = \begin{bmatrix} \sigma_m & 0 & 0 \\ 0 & \sigma_m & \tau_{\theta z} \\ 0 & \tau_{\theta z} & \sigma_m \end{bmatrix} \quad \text{where } \sigma_m = \frac{1}{3} (\sigma_r + \sigma_\theta + \sigma_z)$$

The confining pressure is expressed by the hydrostatic stress tensor. The deviatoric tensor for this case is

$$\bar{\tau} = \begin{bmatrix} 0 & 0 & 0 \\ 0 & 0 & \tau \\ 0 & \tau & 0 \end{bmatrix} \quad \text{where } \tau = \tau_{\theta z}$$

and the shearing strain-rate tensor is

$$\bar{e} = \begin{bmatrix} 0 & 0 & 0 \\ 0 & 0 & \dot{\gamma} \\ 0 & \dot{\gamma} & 0 \end{bmatrix} \quad \text{where } \dot{\gamma} = \dot{\gamma}_{\theta z}$$

Treating the saturated clay as incompressible,

$$e_r = e_\theta = e_z = \dot{\gamma}_{r\theta} = \dot{\gamma}_{zr} = 0$$

In the torsion test of a hollow cylindrical specimen, the state of stress within the specimen can be decomposed into a purely deviatoric state and a purely hydrostatic state. The influence of confining pressure (expressed by the mean normal stress) on the shearing resistance (expressed by the deviatoric state of stress) of soils may be conducted by varying the confining pressures. More importantly, by varying the shearing strain-rate, the rheological equation of state for clay may be determined experimentally with equation (2). An experimental procedure is described in the following section for measuring the shearing stress and shearing strain-rate of a clay sample.

## TORSION TEST METHOD

The main objective of this study was to devise an experimental method by which soil flow properties could be measured by subjecting the soil specimen to a uniform and pure state of stress introduced torsionally. The requirements for the test method are:

1. Develop a rotating testing device capable of applying an instantaneous step-loading on the sample.
2. Acquire equipment to measure the magnitude and speed of the applied torque, and the angular velocity of the sample.
3. Provision for varying the confining pressure on the sample by modifying and adapting an existing triaxial cell.
4. Sample preparation technique for making thin-wall hollow cylinder soil samples.

Since it is difficult to measure directly the shear stress and strain within the sample, in this experiment the applied torque was measured by a torque transducer and shearing strain-rate was determined from the angular velocity.

### A. Torsion Apparatus

Figure 2 shows a schematic and Figure 3 shows photographs of the torsion apparatus and its measuring systems. In this apparatus, the flywheel was rotated at a certain speed and the torque applied instantaneously to the sample by a clutch system. A transducer, identified on the figure, measured the torque.

The flywheel, weighing 356 newtons, was supported by a hardened stainless steel shaft which could rotate and move freely vertically by a combination of linear ball bearings and precision ball bearings. The flywheel was driven by an air jet on the turbine and the speed of rotation measured by a magnetic counter. At the lower end of the flywheel shaft, a spring-loaded tempered-steel jaw was released

by a mechanical clutch, which when engaged to the torsional shaft, applied an instantaneous torsional moment on the specimen in the triaxial chamber at the same rate of angular rotation as the flywheel. The angular rotation of the specimen is also measured with a magnetic counter. The clutch served two important functions: while it rapidly engaged the flywheel to the torsional shaft, it also rapidly disengaged the torsional shaft from the flywheel after the specimen had been rotated 90°. The disengagement prevented any damage to the torque-sensing system inside the triaxial chamber.

A standard triaxial chamber was modified to contain the cylindrical sample. The sample was held firmly at the base, and the top of the specimen connected to the torsional shaft, which had to be fitted precisely to the chamber housing of the triaxial cell. This tight fit which is required to contain the hydrostatic pressure in the chamber, developed substantial friction between the chamber housing and the shaft. To eliminate the effect of the friction, a specially-constructed torsion transducer was mounted between the shaft and the top of the sample cap. The electrical leads of the transducer were packed inside the shaft, which also served as an electrical connector for the transducer. The leads left the shaft outside the triaxial chamber.

#### B. Sample Preparation Unit and Procedure

The size of the sample used in this study was 7.62 cm high with a 1.27 cm-thick wall, having inside and outside diameters, respectively, of 7.62 cm and 10.16 cm. The rapid application of a torsional moment on the hollow clay specimen created a bonding problem between the top and bottom loading caps and the sample. The problem was solved by consolidating the hollow clay sample with the top and bottom loading caps in place.

The dry clay powder was mixed with the proper amount of distilled water and the mixture was allowed to soak for 24 hours. The slurry, at water contents varying between 70% and 80%, was thoroughly mixed and placed in the consolidation mold through a funnel. The consolidation mold (see fig. 4) consisted of a split cylinder with 10.16 cm

internal diameter forming the outside mold, and a solid core cylinder of 7.62 cm diameter forming the inside mold. A bottom cap, which served as the bottom loading cap of the sample, and a top cap, which served as the top loading cap of the sample, completed the mold. The inside face of the split cylinder and the surface of the solid core cylinder were lined with paper cloth which served as an effective filter during the consolidation process for drainage under radial flow. The vertical compression of the sample was achieved by applying a vertical force on the top cap through a rigid piston driven by a pneumatic jack. By gradually varying the vertical consolidation pressure for approximately 48 hours, a hollow cylindrical sample, with the top and bottom loading caps in place, was ready for testing. Figure 5a shows a sample mounted on the base of the triaxial chamber with the torsion transducer placed on the top loading cap. The horizontal wrinkle lines on the sample were formed by the vertical movement of the paper cloth, but these lines did not influence the shearing resistance of the sample. Figures 5 and 6 show various deformed shapes of the sample after the tests were completed.

Mississippi Buckshot Clay was used for all the tests. This was the same type of clay used in the test beds at NASA (refs. 2 and 3) for the measurement of drag loads on an aircraft tire during high-speed operations in clay soil. Figures 7 and 8 show the gradation curve and the compaction characteristics given in reference 2. The consistency limits of the clay (CH) given in reference 2 are:

Liquid Limit	61%
Plastic Limit	28%
Plastic Index	33%

The dry clay powder used in the sample preparation passed through a U.S. Standard No. 12 sieve with 1.651 mm openings.

The water content of the samples for the torsion tests varied from 30.1 to 34.5%, with a dry density corresponding to 14,562 and

13,682 newtons per cubic meter. The average water content of a sample was determined at the end of the test from a total of nine water content measurements, with three each being taken from the top, middle, and bottom of the sample. Some typical results are given in Table 1. The variation of water content in the sample shown is  $\pm 1.2\%$ .

### C. Testing Procedure

At the end of the consolidation period, the inner solid core was removed by a hydraulic jack. With the split cylinder opened, the layers of paper cloth on the inner and outer surface of the cylinder were removed. The sample was seated on the triaxial cell base and the torsion transducer unit was mounted on the top cap. With the triaxial chamber completely assembled and placed in the torsion apparatus, the torsional shaft was connected to the torque transducer shaft by the coupler. The rotation of the sample was measured from the coupler by a magnetic pickup (see figs. 2 and 3).

By regulating the air pressure, the air nozzle turned the flywheel unit until it reached a steady rotation indicated by the magnetic pickup. The clutch was rapidly engaged by lowering the clutch handle and the test was completed in a very short time. The specimen was subjected to an almost instantaneous increase of angular rotation of the same magnitude as that of the flywheel, since the mass ratio between the flywheel assembly and the specimen assembly (including the torsion transducer) was 30 to 1.

The electrical output from the torsion transducer was amplified and recorded on a direct-write oscillograph. The outputs of the magnetic pickup were fed directly to the oscillograph. All tests in this study were conducted with zero confining pressure.

Typical test results are shown in Figure 9. The top trace indicates the angular rotation of the flywheel. With 80 peaks per revolution, the angular velocity is determined from the time pulses, which were set at 0.1-second intervals. The next lower trace indicated the angular rotation of the specimen. The lowest

trace recorded the signal from the torsion transducer. Just before and after the test, a calibration signal from the balancing unit was electronically induced. The calibration signal represented a torque of 4.86 joule. The same magnitude of the calibration signal before and after the test indicated the stability of the electronic system.

#### ANALYSIS OF DATA

Figures 5b, 5c and 6 show some typical final shapes of the soil sample at the end of a test. It was gratifying to note that none of the tests showed any bond failure between the soil sample and the loading plates. As expected, samples with low density (high water content) would deform with the characteristic torsional twist (figs. 5c or 6a), whereas samples with higher density (low water content) would deform with a diagonal brittle fracture (figs. 5b or 6b).

The test results for the torsional resistance (see fig. 9) reflect the combined shearing resistance of the soil and the inertia effect of the transducer and top cap loading plate. In the absence of an analytic solution to separate these effects, it was necessary to conduct dynamic tests to isolate the resistance due to the inertia of the measuring system. A series of inertia tests were conducted by supporting the torsion transducer in the triaxial chamber with ball bearings. A dummy block secured at the base of the triaxial chamber raised the transducer to approximately the same height as during the shear tests. The dynamic response due to inertia effects indicated a linear relationship between the shearing resistance (from inertia) and the angular velocity (see fig. 10).

The shearing resistance of the hollow soil specimen was then determined from the difference of the shear test results and the inertia test results at the corresponding angular velocity of the top loading plate.

The shearing stress distribution of a hollow cylinder due to an applied torque is well established (ref. 11) for the case where the elastic limit of the material is not exceeded. The shearing stress distribution after the elastic limit is exceeded is nonlinear. Since all tests were conducted in this study with zero confining pressure, the shearing elastic limit in clay is very much smaller than the ultimate shearing stress. Furthermore, for a thin-wall hollow cylinder, the stress distribution is very nearly the same in the plastic range. To establish the shearing resistance-strain rate ( $\tau - \dot{\gamma}$ ) diagrams in this study, the clay is treated as an ideally plastic solid.

The relationship between the measured torque and the maximum shearing stress in the hollow cylinder sample is (from the Appendix)

$$\tau_{\max} = \frac{3}{2\pi} \frac{T}{(r_2^3 - r_1^3)} \quad (3)$$

The relationship between the shearing strain-rate at the sample and the angular velocity at the top of the sample (the bottom of sample is fixed), for large deformation is (see Appendix)

$$\dot{\gamma} = \frac{rh}{h^2 + r^2\phi^2} \frac{\delta\phi}{\delta t} \quad (4)$$

For a thin-wall hollow cylinder, the strain-rate is assumed to be the same across the sample so that the mean radius is used in equation (4).

$$r = \frac{1}{2} (r_1 + r_2)$$

All the test results (see fig. 9) indicated that the maximum torque was recorded at an angular displacement at the top of the sample of  $\phi = 0.07$  radians ( $4.5^\circ$ ). The second term in the denominator of equation (4) is neglected and equation (4) is reduced to

$$\dot{\gamma} = \frac{r}{h} \frac{\delta\phi}{\delta t} \quad (5)$$

Since the sample was torqued very rapidly through a large flywheel, the angular velocity of the top of sample was almost the same as the angular velocity of the flywheel during the initial period when the maximum torque was developed. The strain-rate of the specimen was determined from the angular velocity of the flywheel using equation (5).

The tests were conducted for a range of water content in a saturated, undrained state. Since the variation of water content in each specimen was  $\pm 1.2\%$ , the test results were analyzed for water content in the following four groups:

30% < w < 31%	mean water content = 30.5%
31% < w < 32%	mean water content = 31.5%
32% < w < 33%	mean water content = 32.5%
33% < w < 34%	mean water content = 33.5%

Figures 9a, 9b and 9c are photographs of typical test results. The applied strain-rates are 4.8, 13.3, and 2.3 rad/sec, respectively. Regardless of the magnitude of strain-rate, all results indicated that the maximum shearing stress occurred at small angular displacements and the shearing stress level is related to the dry density of the clay expressed in terms of water content.

For an applied shearing rate of less than 15 rad/sec, the shearing strain-rate relationship may be expressed by an exponential function which approaches a certain constant stress with strain-rate as (see fig. 11):

$$\tau = \alpha(1 - e^{-\beta\dot{\gamma}}) \quad (6)$$

The value of the coefficient  $\alpha$ , which is equal to the maximum ultimate shearing resistance of the soil, can be found from the

asymptotic shear stress as presented in Figure 11. These values are summarized as a function of mean water content in Figure 12, which shows that  $\alpha$  increases with decreasing water content and appears to be linear in the range between 30 and 33%. Due to lack of experimental results, it cannot be explained why the value of coefficient  $\alpha$  becomes constant at higher water contents.

The value of coefficient  $\beta$  in equation (6) can be found by plotting strain-rate as a function of  $\log (\alpha - \tau)$  since the logarithm of that equation yields

$$\gamma = \frac{2.3}{\beta} \log \alpha - \log (\alpha - \tau) \quad (7)$$

This relationship is presented in Figure 13. The magnitude of  $\beta$  is the slope of the resulting curve and equals 0.35 regardless of the water content range. The  $\alpha$  and  $\beta$  for various dry density and water content are summarized in Table 2.

The experimental results demonstrated the non-viscoelastic response of the clay under dynamic loading. The relationship between stress and strain-rate cannot be described by a simple constant such as a Newtonian viscosity. Since the shear stress approaches a maximum value as the strain-rate increases (within the test range covered in this investigation) the clay behaved as a pseudoplastic or shear-thinning body. This non-Newtonian flow behavior is often described by an apparent viscosity (ref. 12) where

$$\eta_{app} = f(\tau, \dot{\gamma})$$

Figure 14 gives a typical plot of apparent viscosity as a function of strain-rate.

The apparent viscosity is adopted in many engineering applications. The apparent viscosity increases linearly with increasing dry density. For each dry density, the apparent viscosity decreases as the strain-rate increases, as shown in the figure. This decrease

results in reduced energy requirements in many engineering applications. For instance, in the problem concerning aircraft operation on soil runways, the reduced energy requirement implies a lower drag on the landing gear. In the problem concerning earth moving and tillage industries, the energy requirement reduction is important to the design and operation of the equipment.

#### SUMMARY AND CONCLUSIONS

1. A new experimental method for studying the effect of rate of shearing on the shearing resistance of cohesive soils has been presented in this investigation.

2. The equation of state relating the ultimate shearing resistance to the strain-rate can be described. The pseudoplastic behavior cannot be described with linear rheological models.

3. The rheological coefficient  $\alpha$  varies linearly with the dry density of the clay to a certain lower limit and remains constant as the dry density decreases.

4. The rheological coefficient  $\beta$  is constant for the clay.

5. For a given dry density, the apparent viscosity decreases with increasing strain-rate.

6. The influence of the mean normal pressure on the rheological properties of clay is not included in this study.

#### ACKNOWLEDGMENT

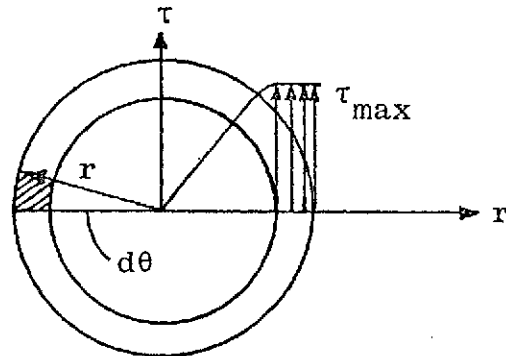
The author wishes to express his appreciation to Mr. Trafford J.W. Leland of NASA-Langley Research Center, for his constant advice and assistance throughout this study.

## REFERENCES

1. Wismer, R.D.: Performance of Soils Under Tire-loads. Rep. 3 - Tests in Clay Through No. 1962. Tech. Rep. No. 3-666, U.S. Army Eng. Waterways Exp. Sta., Corps Eng., February 1966.
2. Crenshaw, B.M., Butterworth, C.K., and Truesdale, W.B.: Aircraft Landing Gear Dynamic Loads from Operation on Clay and Sandy Soil. AFFDL-TR-69-51, U.S. Air Force, February 1971.
3. Leland, T.J.W., and Smith, E.G.: Aircraft Tire Behavior During High-speed Operations in Soil. NASA TN D-6813, August 1972.
4. Karatiath, L., and Nowatzki, E.A.: The Effect of Speed on Wheel Drag in Soil, Grumman Research Department, Memorandum RM-546, July 1972.
5. Leonards, G.A.: Engineering properties of soils, Foundation Engineering, McGraw-Hill Book Company, 1962.
6. Wu, T.H. Soil Dynamics, Allyn and Bacon, Inc. 1971.
7. Atakol, K. and Larew, H.G.: Experimental Studies of the Transient Strength-Deformation Characteristics of Soil, Report No. CE-4877-102-670, University of Virginia, June 1967.
8. Hendrick, J.G., and Gill, W.R.: Soil Reaction to High Speed Cutting, ASAE, Vol. 16, No. 3, 1973, pp. 401-403.
9. Geuze, E.C.W.A., and Tan, T.K.: The Mechanical Behavior of Clays, Proceedings of 2nd International Congress of Rheology, 1954.
10. Saada, A.S., and Ou, C.D.: Strain-Stress Relations and Failure of Anisotropic Clays, J. of the Soils Mechanics and Foundation Division, ASCE, Vol. 99, SM12, December 1973.
11. Timoshenko, S.P., and Gere, J.M.: Mechanics of Materials, Van Nostrand Reinhold Company, 1972.
12. Maxwell, B.: The Dynamic Behavior and Stress Relaxation of Polymer Melts, Polymer Engineering and Science, Vol. 8, No. 4, 1968.

## APPENDIX

(A) Relationship between shear stress and applied torque in the plastic range.



$r = r_1$  inside radius  
 $r = r_2$  outside radius

In the plastic state, the shear stress across the cylinder wall is considered to be constant. Considering the equilibrium condition that the applied torque is equal to the total internal twisting moment, yields

$$\begin{aligned}
 T &= \int_A \tau_{\max} r \, dA \\
 &= \int_{r_1}^{r_2} \int_0^{2\pi} \tau_{\max} r^2 d\theta \, dr \\
 &= \frac{2\pi}{3} (r_2^3 - r_1^3) \tau_{\max}
 \end{aligned}$$

or

$$\tau_{\max} = \frac{3}{2\pi} \frac{T}{(r_2^3 - r_1^3)}$$

(B) Relationship between strain-rate and angular velocity from figure 1,

$$\gamma = \tan^{-1} \left( \frac{r\phi}{h} \right)$$

$$\frac{\delta\gamma}{\delta t} = \dot{\gamma} = \left( \frac{rh}{h^2 + r^2\phi^2} \right) \frac{\delta\phi}{\delta t}$$

For  $\phi \leq 7^\circ$  and small values for  $r$ , the second term in the denominator of the right hand side may be neglected and  $\dot{\gamma}$  may be expressed by

$$\dot{\gamma} = \frac{r}{h} \frac{\delta\phi}{\delta t}$$

Table 1

Water Content at Various Locations on a Typical Sample

Location on Sample	Water Content, %		
	A	B	C
Top	30.1	30.3	29.6
Middle	30.5	31.0	30.2
Bottom	28.7	29.5	29.0
Average	29.9 ± 1.2		

Table 2

Values of Coefficients  $\alpha$  and  $\beta$

Mean Water Content %	Mean Dry Density $\text{kN/m}^3$	Void Ratio	$\alpha$ dynes/cm <sup>2</sup>	$\beta$ second
30.5	14.49	.84	12	.35
31.5	14.25	.87	9.5	.35
32.5	14.10	.89	6.7	.35
33.5	13.88	.92	6.7	.35

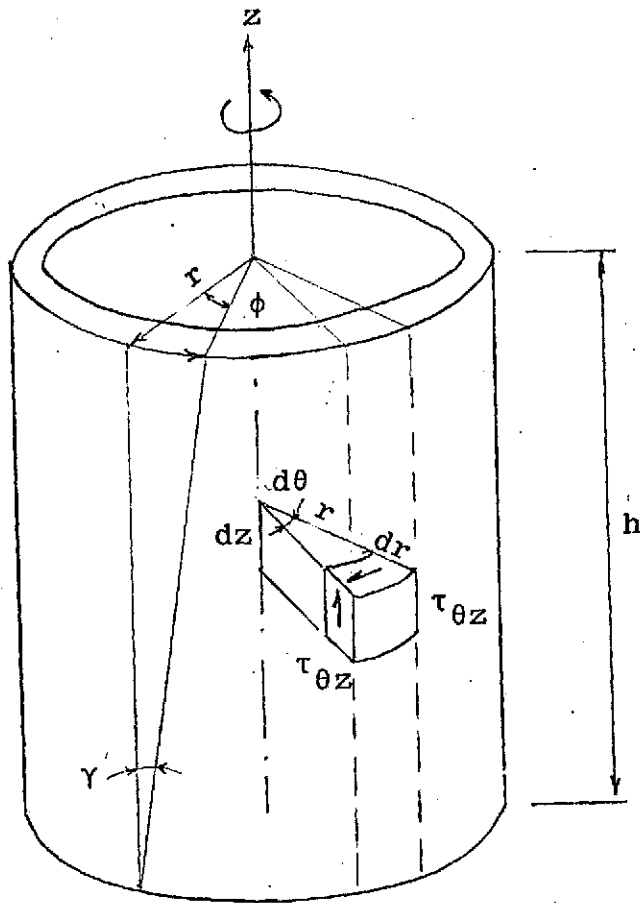
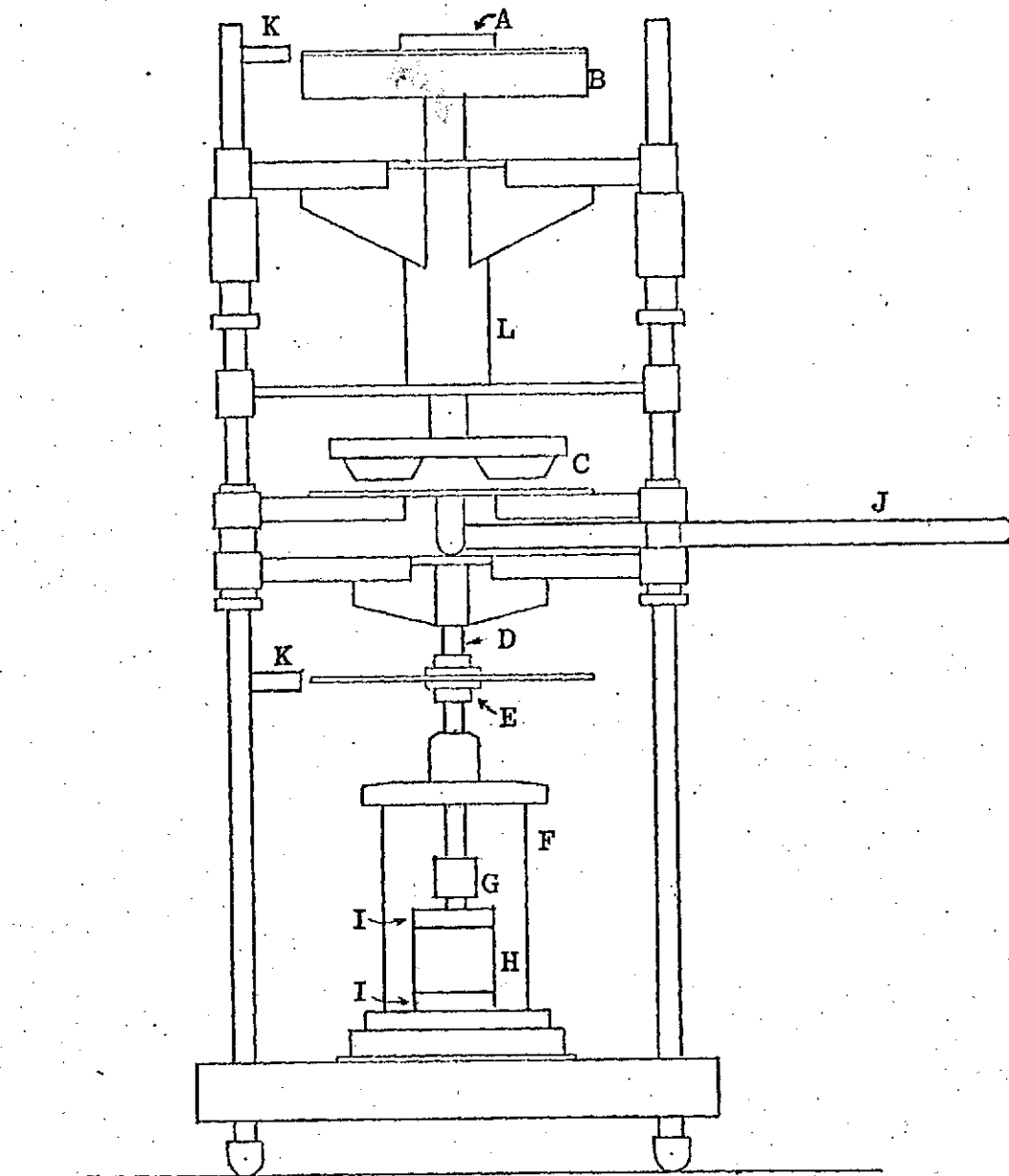


Figure 1. Reference axes and stress system.

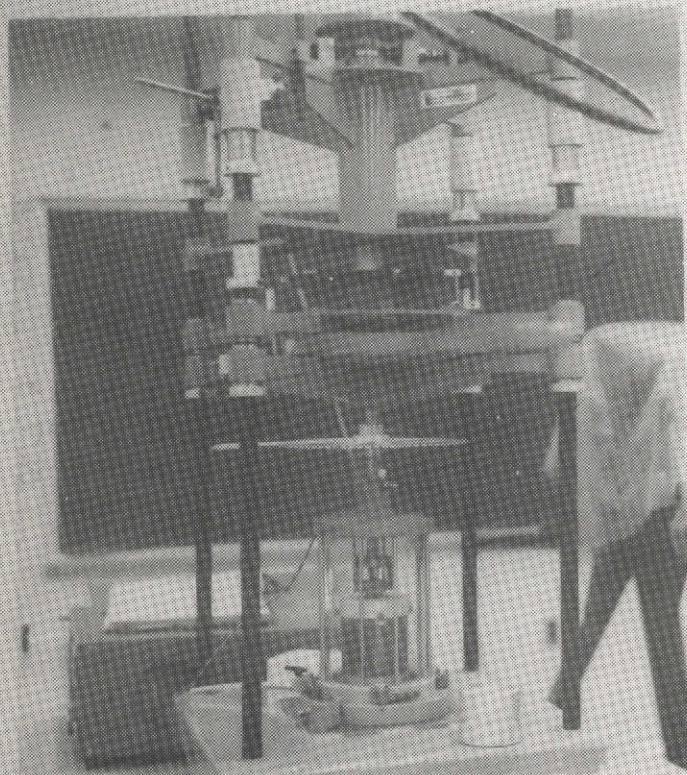
ORIGINAL PAGE IS  
OF POOR QUALITY



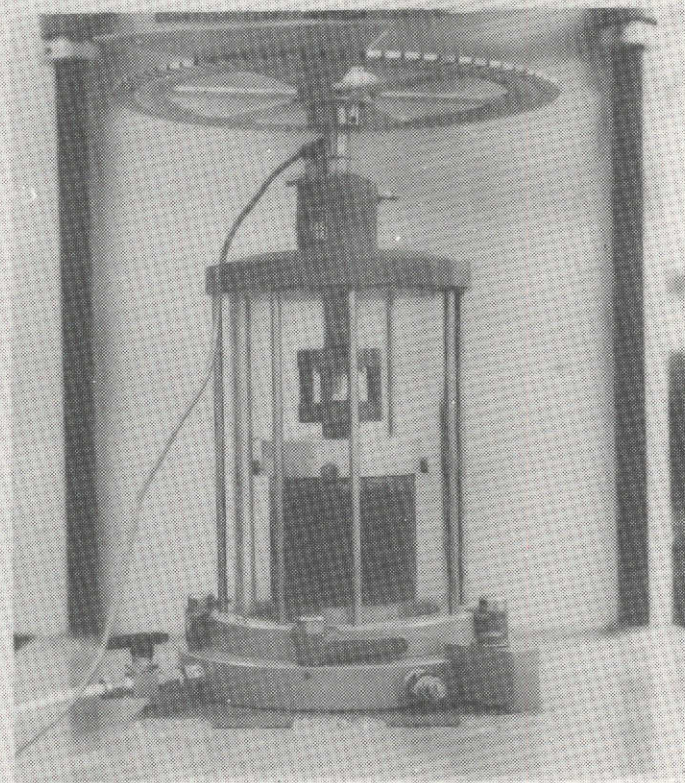
- |    |                 |    |                      |
|----|-----------------|----|----------------------|
| A. | Turbine         | G. | Torque transducer    |
| B. | Flywheel        | H. | Test sample          |
| C. | Clutch assembly | I. | Loading plate        |
| D. | Torsion shaft   | J. | Clutch handle        |
| E. | Coupler         | K. | Magnetic counter     |
| F. | Triaxial cell   | L. | Linear ball bearings |

ORIGINAL PAGE IS  
OF POOR QUALITY

Figure 2. Torsion apparatus.



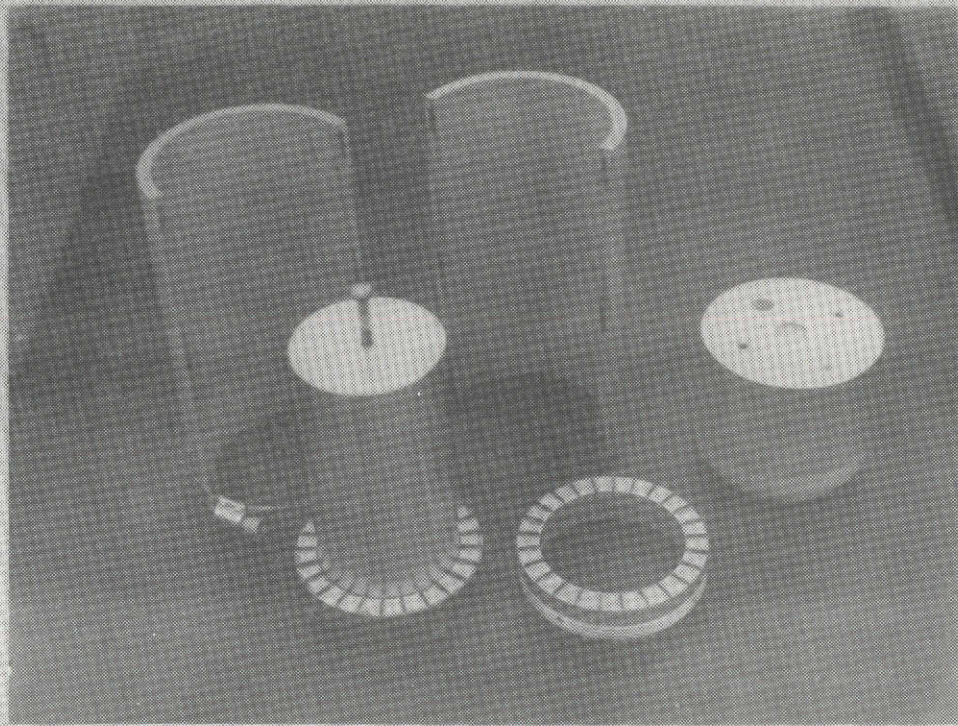
(a) Overall view



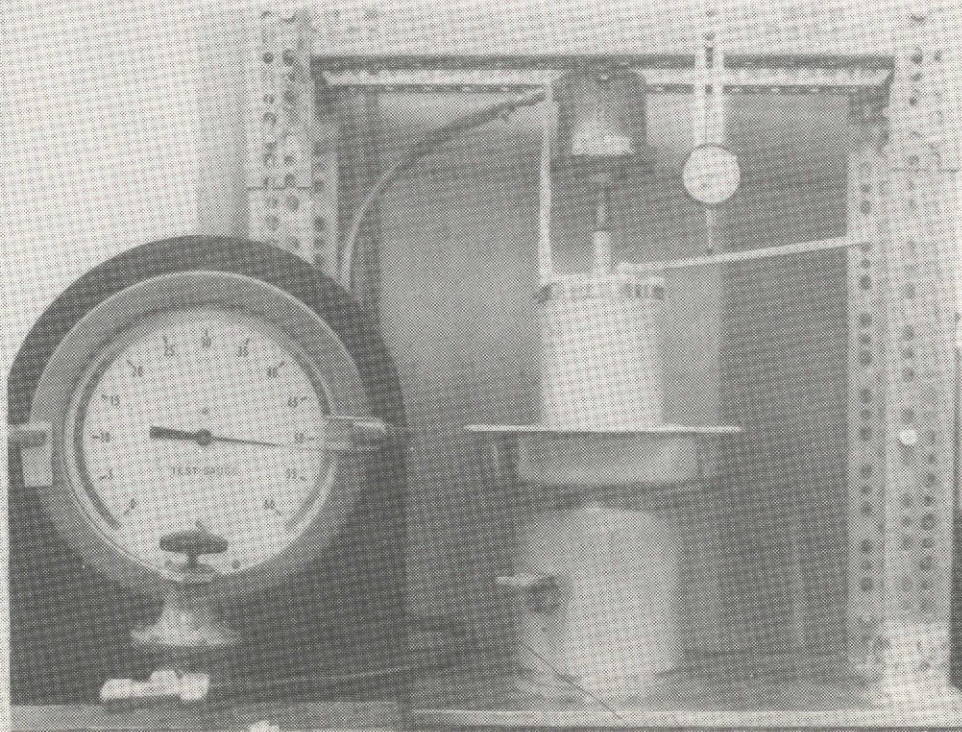
(b) Close-up of sample in triaxial cell

Figure 3.- Photograph of torsion apparatus.

ORIGINAL PAGE IS  
OF POOR QUALITY

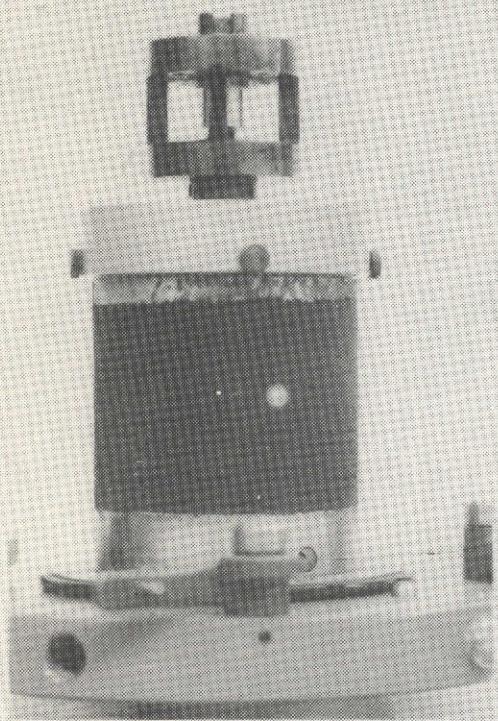


(a) Sample mold

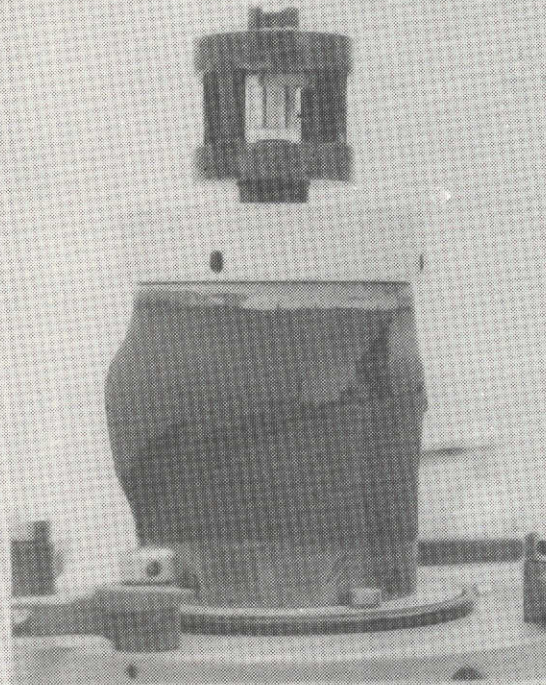


(b) Consolidation apparatus

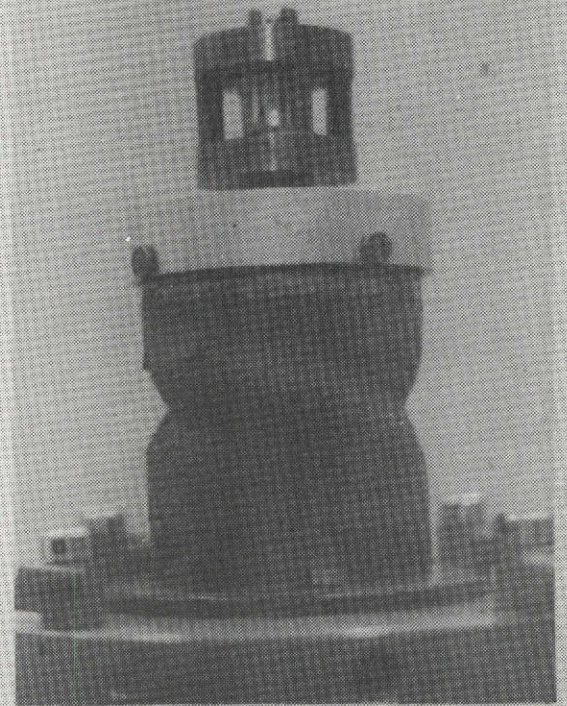
Figure 4.- Photograph of sample preparation unit. ORIGINAL PAGE IS OF POOR QUALITY



(a) Sample before testing



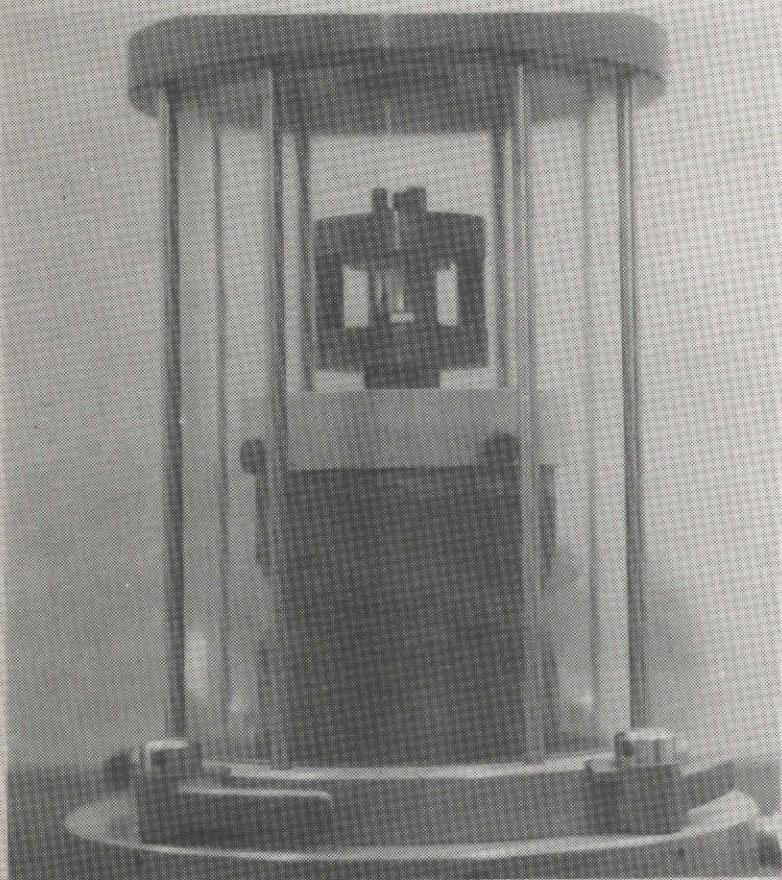
(b) Low water-content  
sample after testing



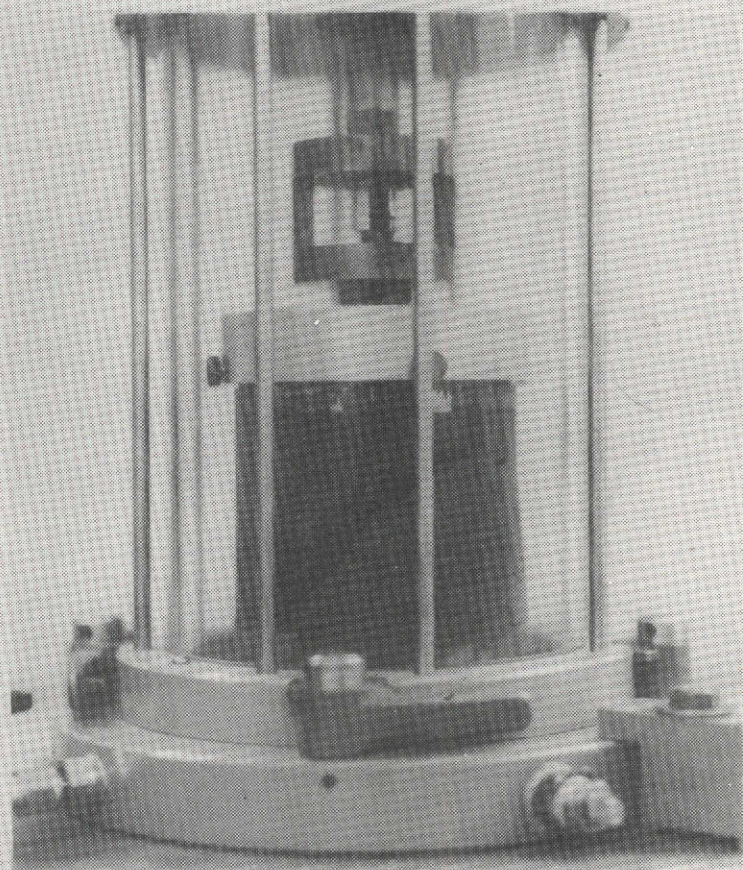
(c) High water-content  
sample after testing

Figure 5.- Photograph of test samples.

ORIGINAL PAGE IS  
OF POOR QUALITY



(a) High water-content sample



(b) Low water-content sample

Figure 6.- Photograph of test sample in triaxial cell.

Hydrometer

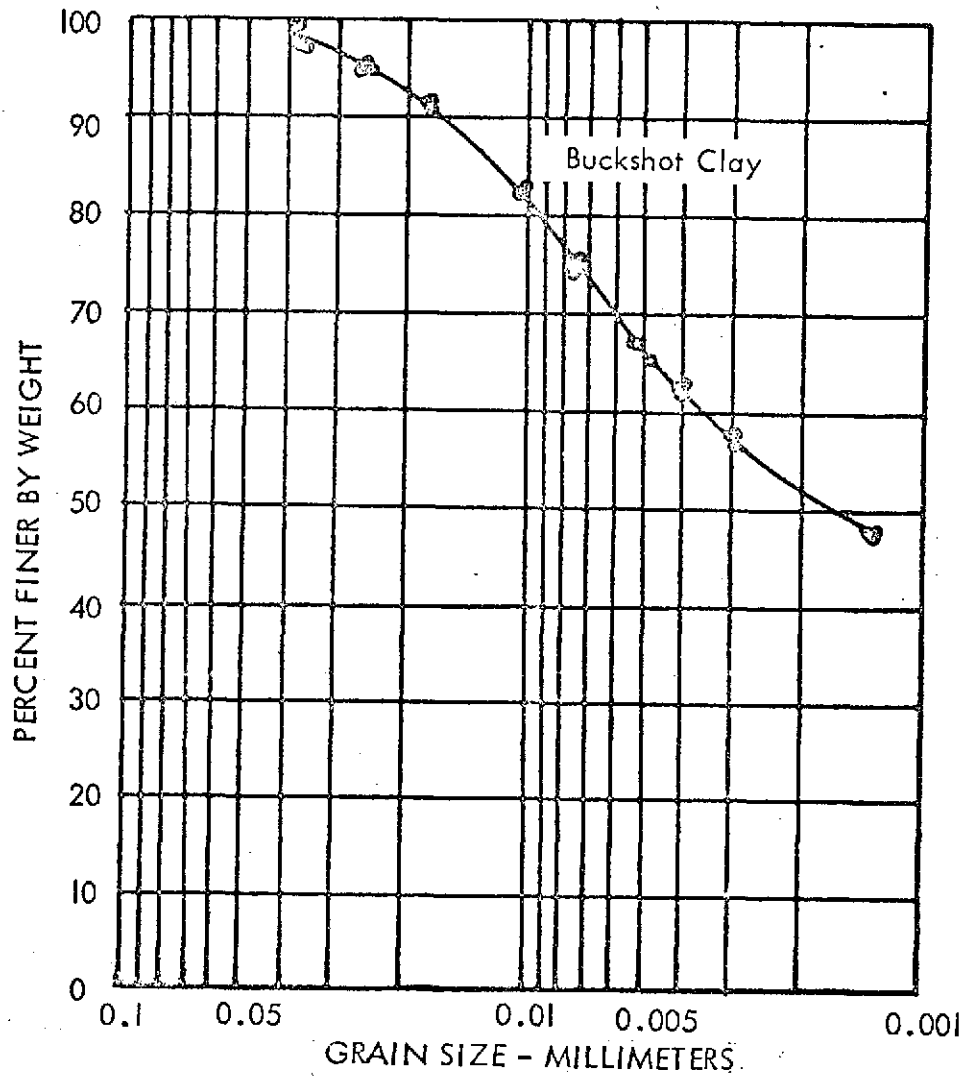


Figure 7. Grain size distribution of clay (ref. 2).

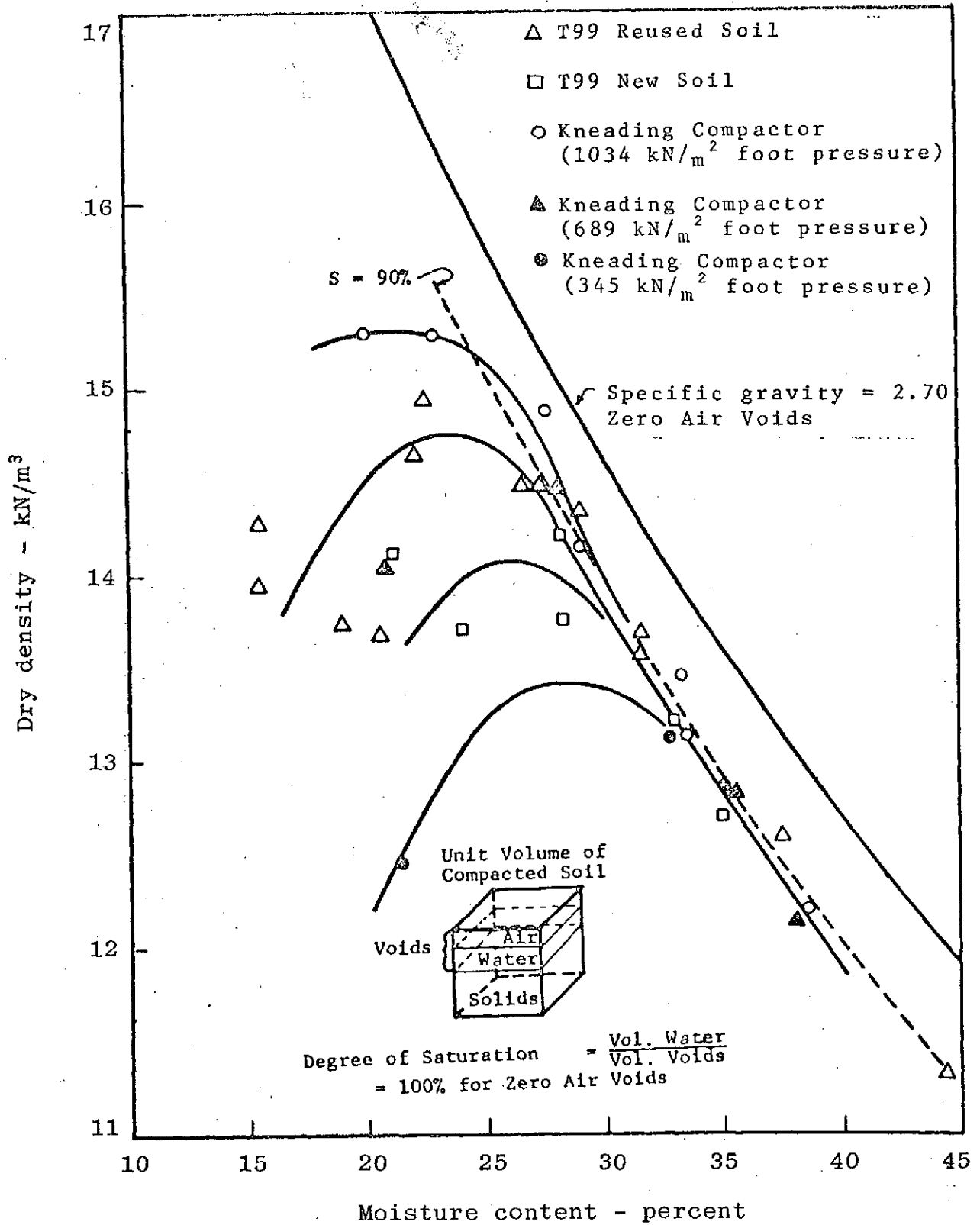
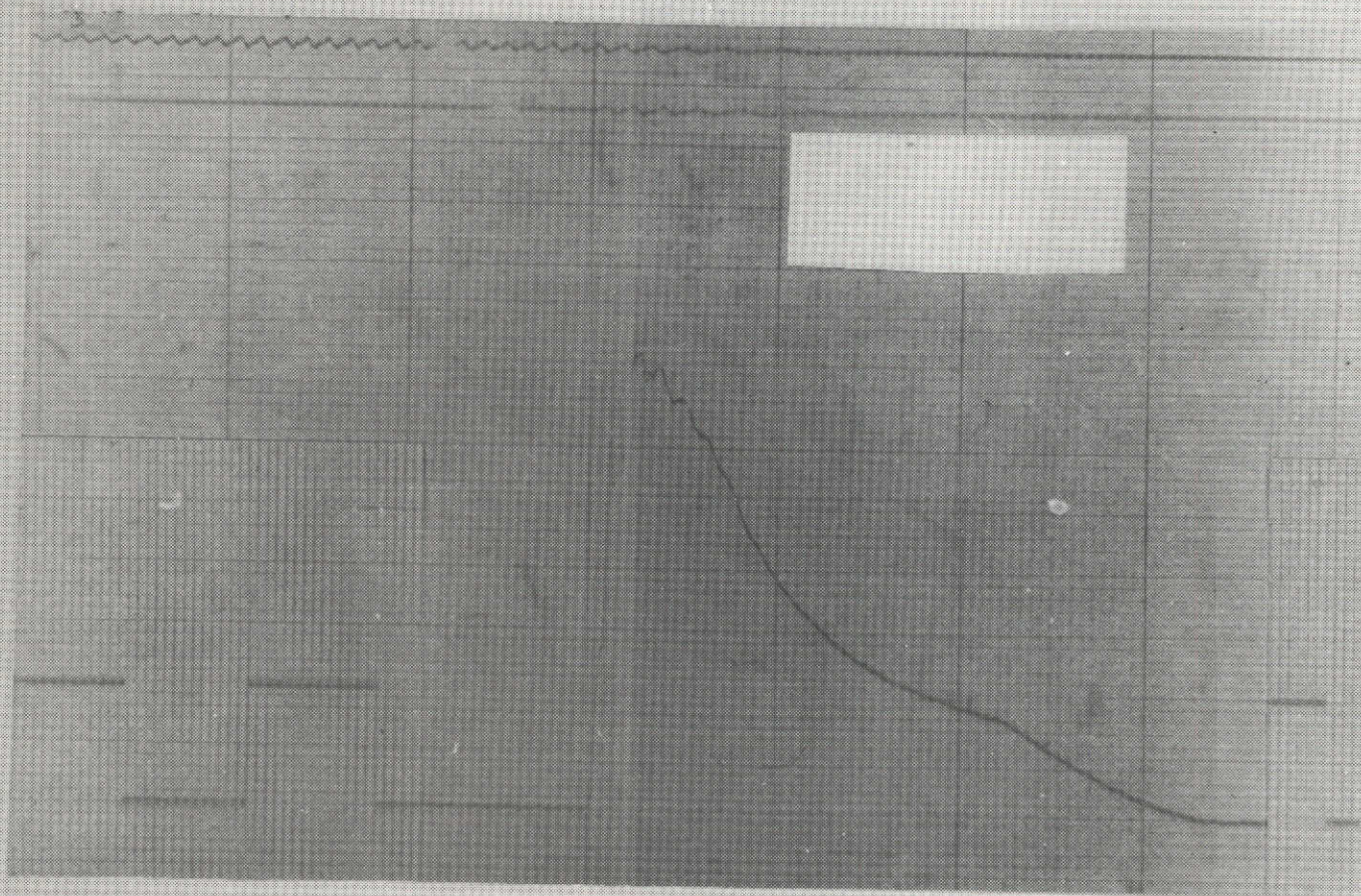
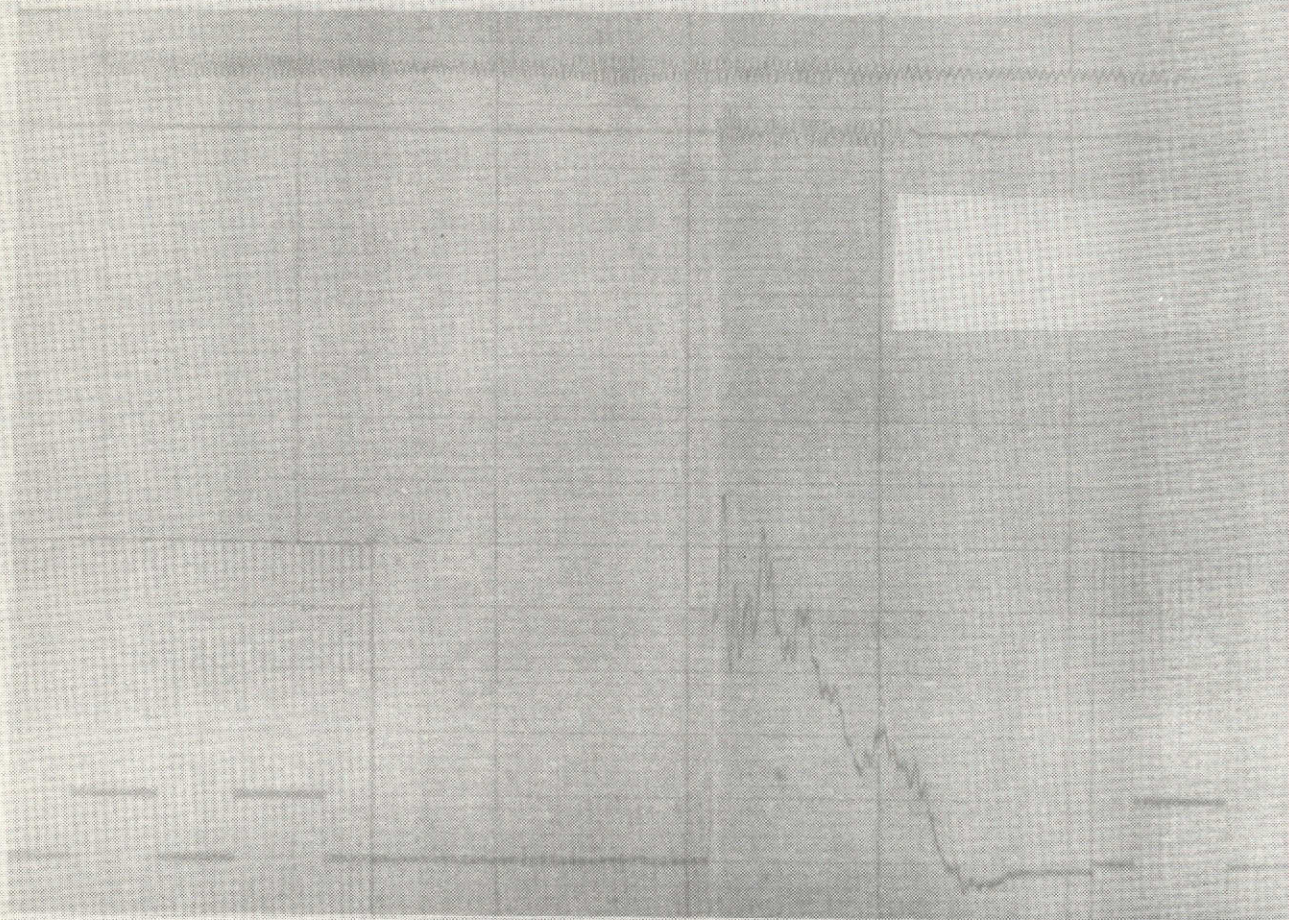


Figure 8. Compaction property of clay (ref. 2).



(a) Water content = 30% ; shearing strain-rate = 4.8 rad/sec.

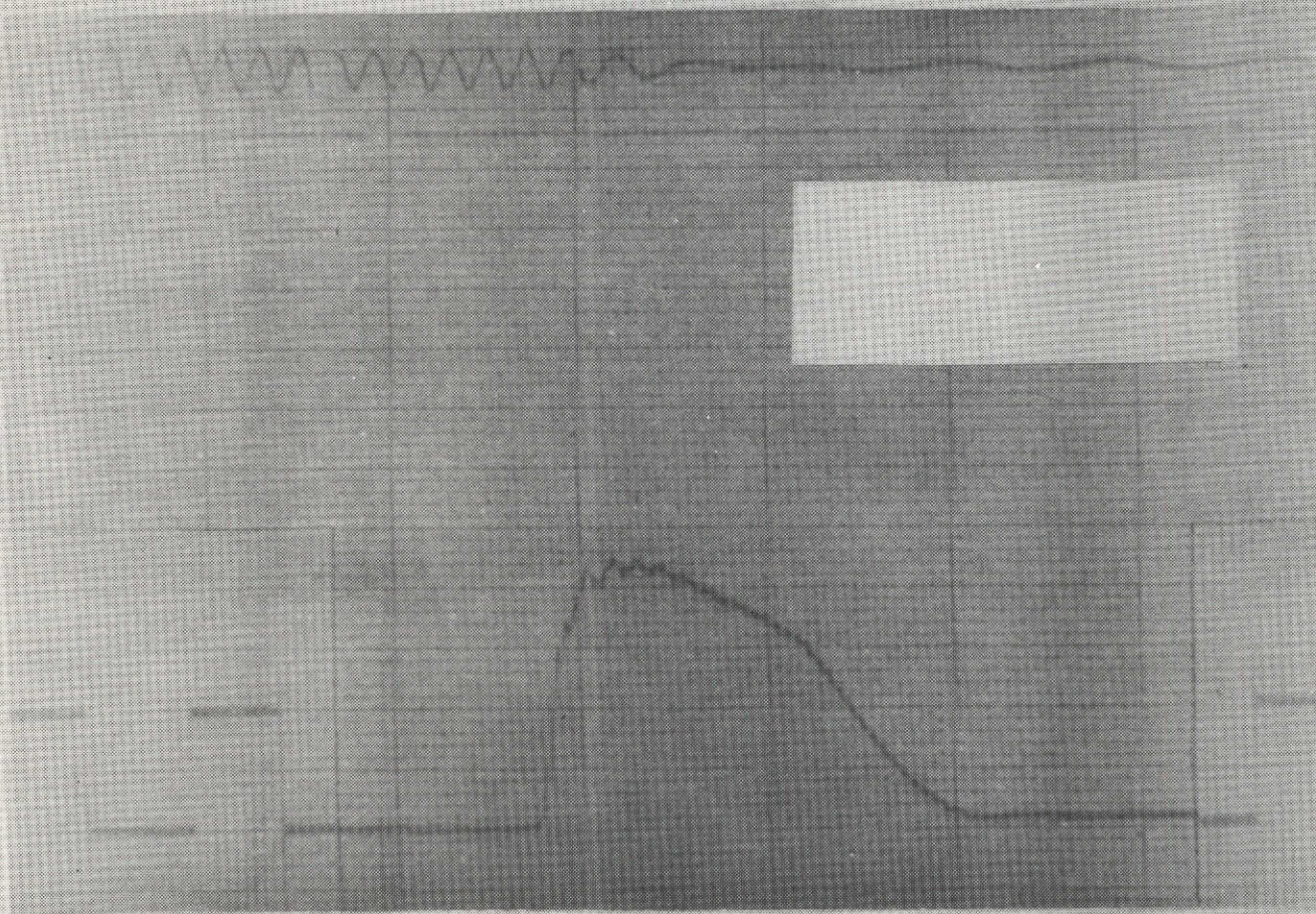
Figure 9.- Photographs of typical recorded time histories.



(b) Water content = 31.3 % ; shearing strain-rate = 13.3 rad/sec.

Figure 9.- Continued.

ORIGINAL PAGE IS  
OF POOR QUALITY



(c) Water content = 32.7 % ; shearing strain-rate = 2.3 rad/sec.

Figure 9.- Concluded.

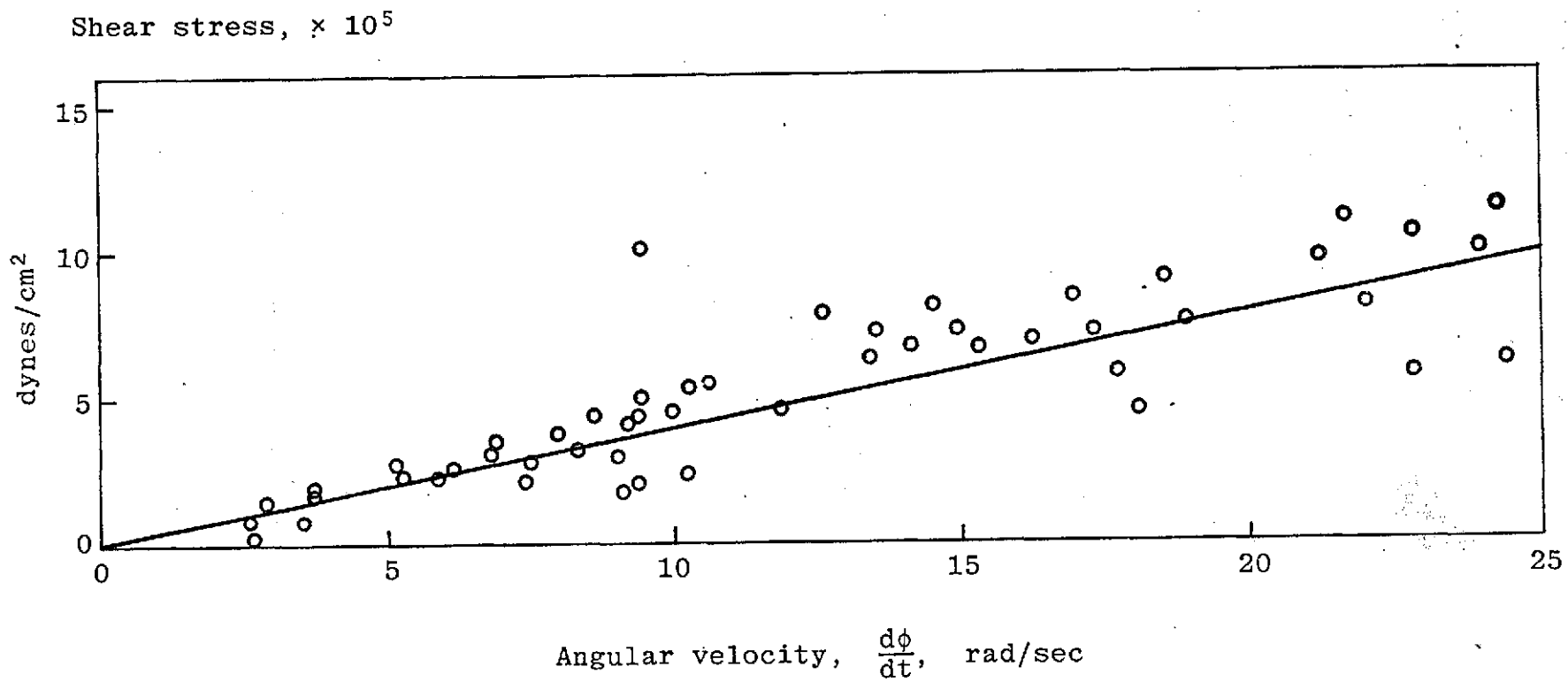


Figure 10. Dynamic response due to inertia of the torque sensing system.

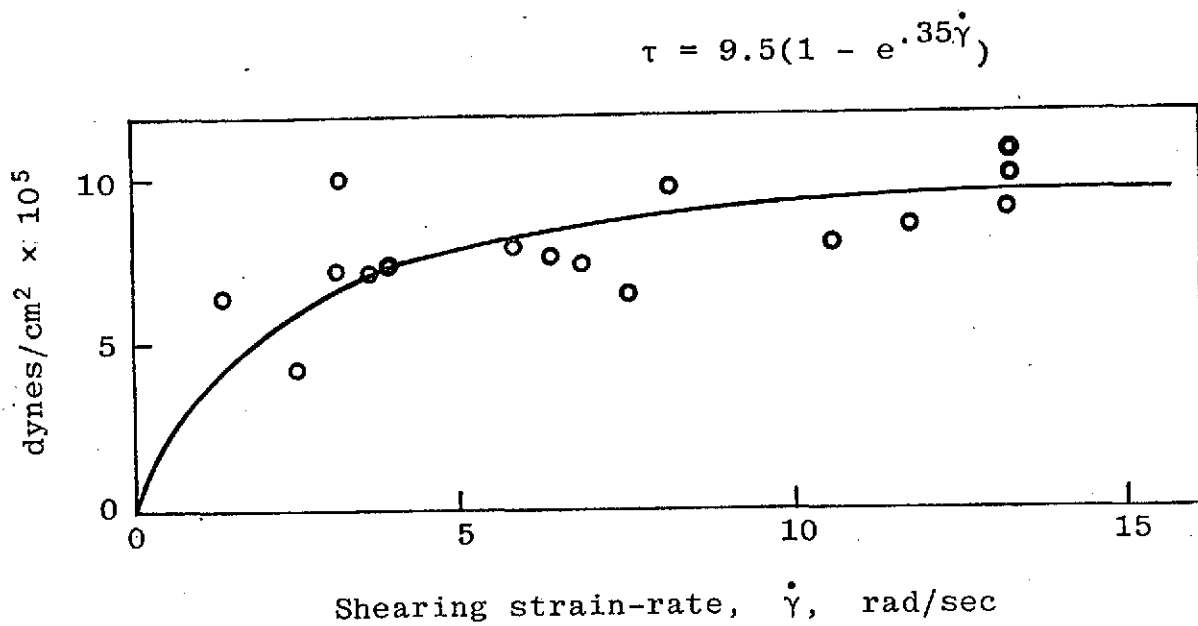
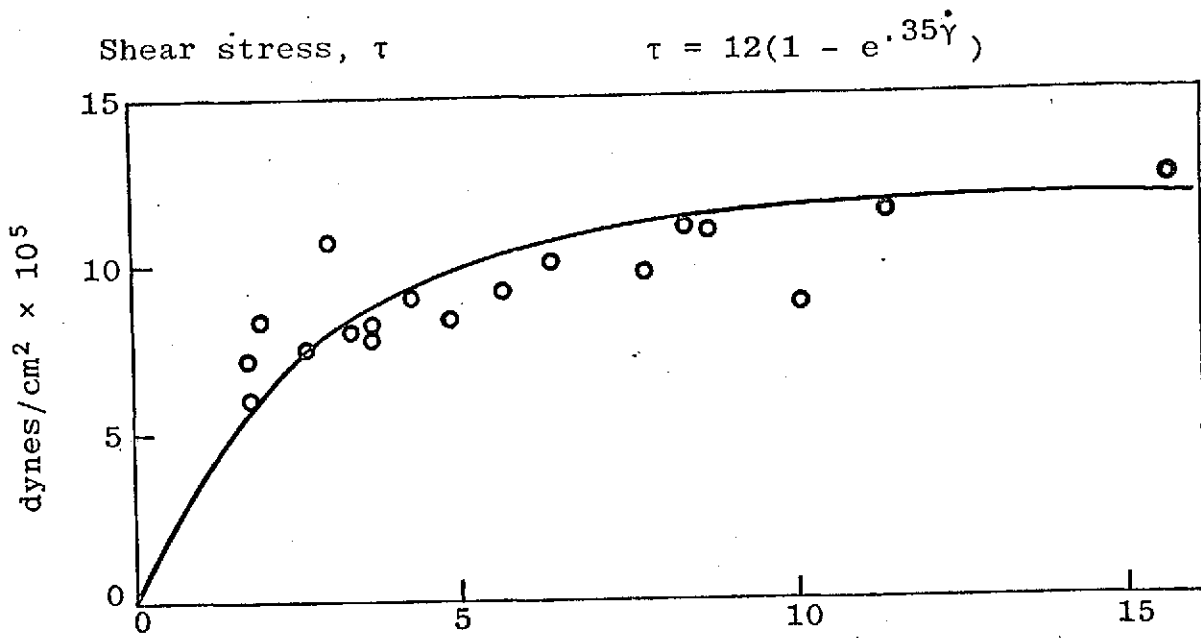
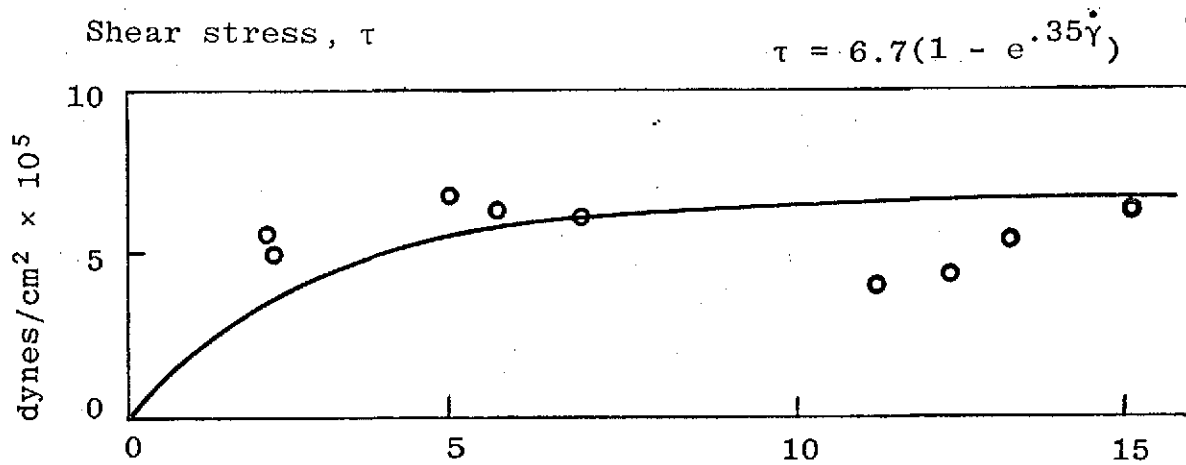
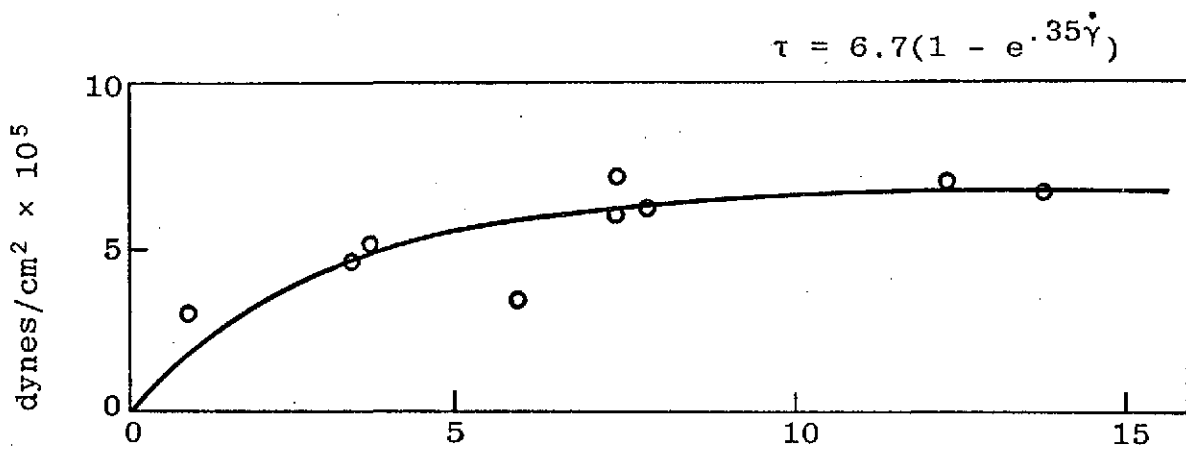


Figure 11. Plot of shearing stress vs. strain-rate.



(c) mean water content = 32.5%



Shearing strain-rate,  $\dot{\gamma}$ , rad/sec

(d) mean water content = 33.5%

Figure 11. Concluded.

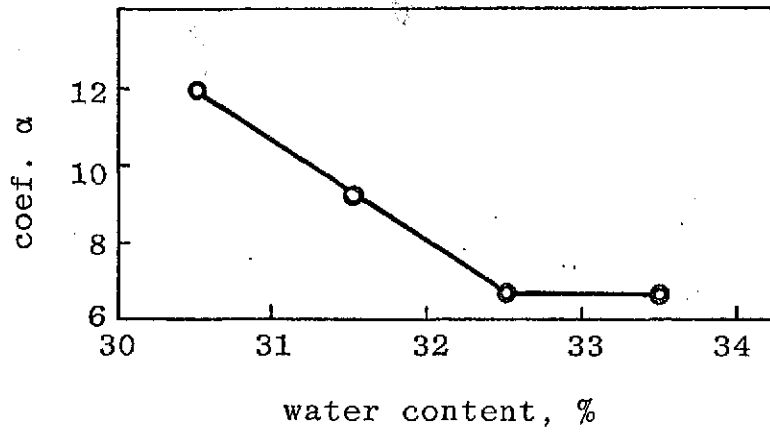


Figure 12. Relationship between coef.  $\alpha$  and mean water content.

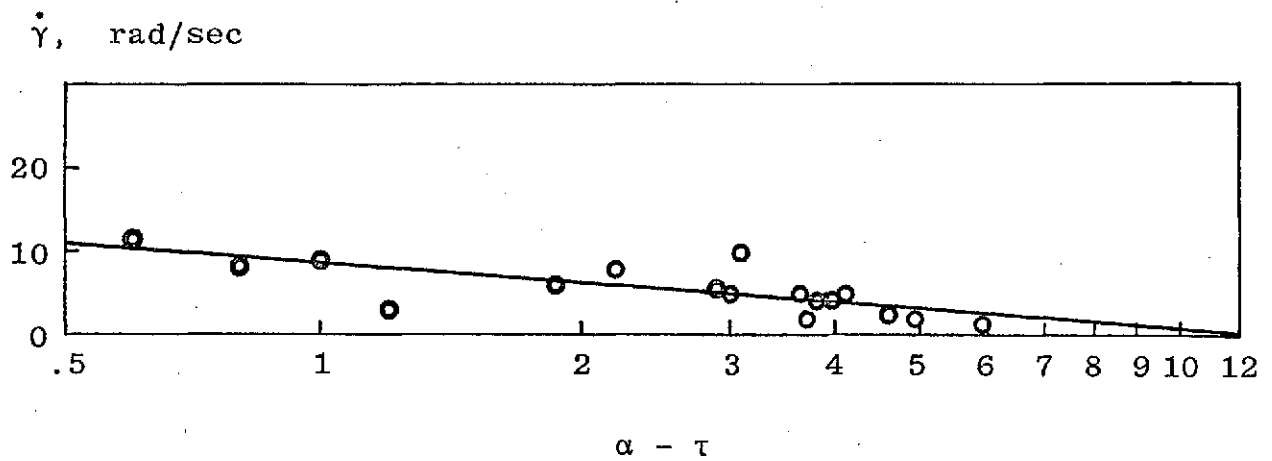
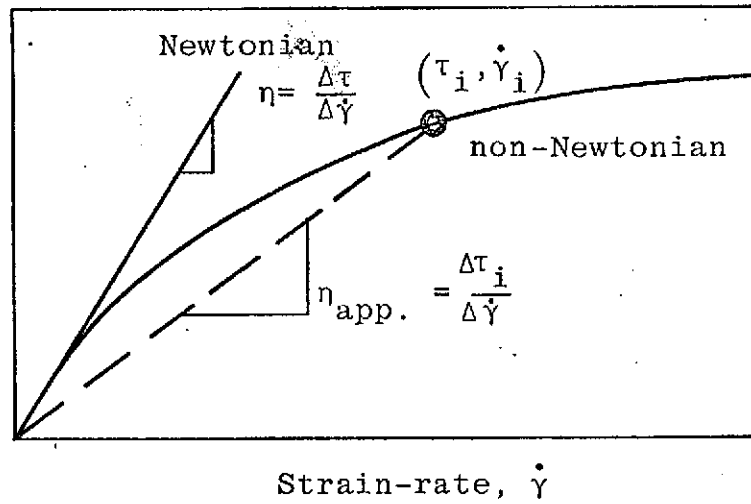
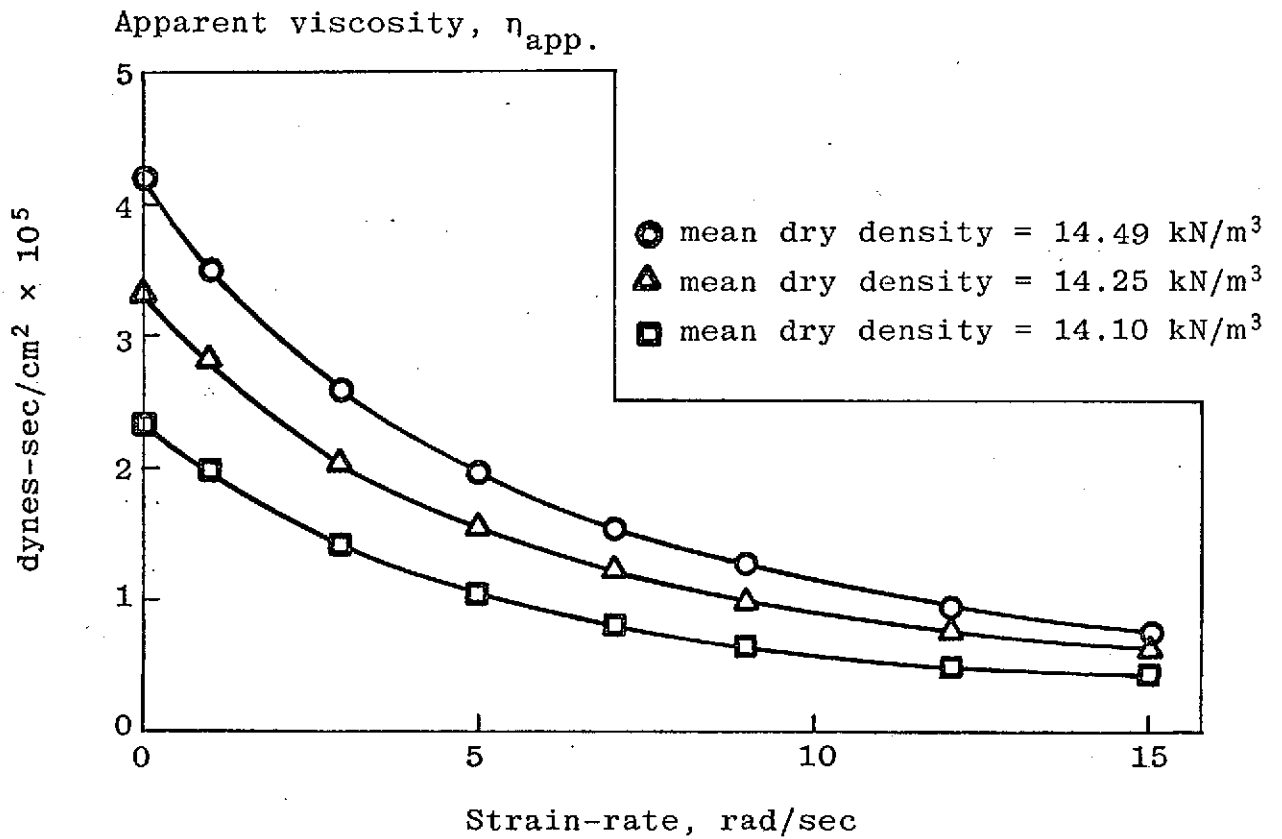


Figure 13. Plot of strain-rate vs.  $\log_{10} (\alpha - \tau)$

Shear stress,  $\tau$



(a) Newtonian and non-Newtonian viscosity



(b) Apparent viscosity vs. strain-rate

Figure 14. Newtonian and non-Newtonian viscosity, and plot of apparent viscosity versus strain-rate.